Metabolic phenotyping of healthy and diseased human RPE cells

Saira Rizwan[1,2*], Beverly Toothman[1,2*], Bo Li[1,2,3*], Abbi J. Engel[4], Rayne R Lim[4], Jinyu Lu[1,2], Jennifer R. Chao[4&], and Jianhai Du[1,2&]

[1]Department of Ophthalmology and Visual Sciences, West Virginia University, Morgantown, WV 26506

[2]Department of Biochemistry and Molecular Medicine, West Virginia University, Morgantown, WV 26506

[3]Department of Ophthalmology, Affiliated Hospital of Yangzhou University, Yangzhou University, Yangzhou, Jiangsu Province 225100, China.

[4]Department of Ophthalmology, University of Washington, Seattle, WA 98109, United States.

[*]Equal contributions

[&]Corresponding Authors: Jianhai Du, One Medical Center Dr, PO Box 9193, WVU Eye Institute, Morgantown, WV 26505; Phone: (304)-293-9346; Fax; (304)-598-6928; Email: jianhai.du@hsc.wvu.edu; or Jennifer R. Chao: 50 Republican Street, Box 358058, Seattle WA 98109; Phone: (206) 221-0594. Email: jrchao@uw.edu.

Word count: 3499

Commercial relationships disclosures: None.

Funding: The funders had no role in the study design, data collection and analysis, decision on publishing, or manuscript preparation. This work was supported by National Institutes of Health Grant EY034364 (J. R. C. and J. D), EY03459 (J. R. C. and J. D), EY031324 (JD), EY032462(JD), the Retina Research Foundation (JD) and funds for Core facilities P20 GM103434 and P20 GM144230 (WV INBRE grant).

Abstract (250 words)

Purpose: Metabolic defects in retinal pigment epithelium (RPE) are underlying many retinal degenerative diseases. This study aims to identify the nutrient requirements of healthy and diseased human RPE cells.

Methods: We profiled the utilization of 183 nutrients in human RPE cells: 1) differentiated and dedifferentiated fetal RPE (fRPE), 2) induced pluripotent stem cell derived-RPE (iPSC RPE), 3) Sorsby fundus dystrophy (SFD) patient-derived iPSC RPE and its CRISPR-corrected isogenic SFD (cSFD) iPSC RPE, and 5) ARPE-19 cell lines cultured under different conditions.

Results: Differentiated fRPE cells and healthy iPSC RPE cells can utilize 51 and 48 nutrients respectively, including sugars, intermediates from glycolysis and tricarboxylic acid (TCA) cycle, fatty acids, ketone bodies, amino acids, and dipeptides. However, when fRPE cells lose epithelial phenotype through dedifferentiated, they can only utilize 17 nutrients, primarily sugar and glutamine-related amino acids. SFD RPE cells can utilize 37 nutrients; however, Compared to cSFD RPE and healthy iPSC RPE, they are unable to utilize lactate, some TCA cycle intermediates, and short-chain fatty acids. Nonetheless, they show increased utilization of branch-chain amino acids (BCAAs) and BCAA-containing dipeptides. The dedifferentiated ARPE-19 cells in traditional culture media cannot utilize lactate and ketone bodies. In contrast, nicotinamide supplementation promotes differentiation into epithelial phenotype, restoring the ability to use these nutrients.

Conclusions: Epithelial phenotype confers metabolic flexibility to the RPE for utilizing various nutrients. SFD RPE cells have reduced metabolic flexibility, relying on the oxidation of BCAAs. Our findings highlight the importance of nutrient availability and utilization in RPE differentiation and diseases.

Introduction

Retinal pigment epithelium (RPE) plays a vital role in supporting photoreceptor function and survival through various specific functions, including visual cycle, nutrient transport, light absorption, phagocytosis of outer segments, and formation of the blood-retina barrier[1]. To sustain these critical functions, the RPE relies on a robust mitochondrial metabolism by oxidizing fuels from the photoreceptors and choroidal supply[2]. Defects in RPE mitochondrial metabolism can cause RPE epithelial-mesenchymal transition (EMT) and dedifferentiation to lose its epithelial characteristics such as tight junctions, pigmentation and polarity, subsequently leading to photoreceptor death in retinal degenerative diseases, including Sorsby Fundus Dystrophy (SFD), and age-related macular degeneration (AMD)[2-4].

Cultured human RPE cells are pivotal to studying RPE function and elucidating mechanisms underlying retinal degenerative diseases[5-7]. The most common types of RPE cultures include human fetal RPE (fRPE), patient-derived induced pluripotent stem cells (IPSC) RPE, and ARPE19. Cultured mature human RPE cells exhibit typical RPE morphology, function and signature gene expression closely resembling native RPE cells[8]. Mitochondrial metabolism regulates RPE nutrient utilization, maturation, morphology and function[5, 9]. For instance, mature fRPE and iPSC RPE cells preferentially oxidize proline to fuel mitochondrial metabolism, a feature positively correlated with RPE maturation. In contrast, dedifferentiated RPE lacks the ability to effectively oxidize proline[10, 11]. ARPE19 cells show fibroblast-like morphology under traditional culture media. However, supplementation with nicotinamide (NAM), a precursor for NAD, can rapidly induce differentiation of ARPE19 cells into RPE cells with many epithelial characteristics through revitalizing mitochondrial metabolism[12, 13].

SFD, a rare macular degeneration caused by mutations in the Tissue Inhibitor of Metalloproteinase-3 (TIMP3) gene, presents clinical manifestations similar to AMD[14]. We demonstrate that iPSC RPE derived from SFD patients carrying the S204C mutation in *TIMP3* reproduces sub-RPE deposits observed in the globes from SFD patients[15]. Employing CRISPR-Cas9 gene editing, correction of the S204C mutation in SFD iPSC RPE (cSFD) diminishes the presence of sub-RPE deposits. Notably, SFD RPE enhances the breakdown of the extracellular matrix (ECM) proteins but increases lipid and protein-rich deposits[15].

In this study, we aimed to elucidate the metabolic phenotype of nutrient utilization in healthy and diseased human RPE. To this end, we conducted an extensive metabolic screening carbon and nitrogen sources across various human RPE cultures, including mature and dedifferentiated fRPE, healthy and SFD RPE, and ARPE19 RPE cells under different culture media. We have found healthy and mature RPE

cells demonstrate robust metabolic flexibility, allowing them to utilize various nutrient sources. In contrast, the dedifferentiated and SFD RPE cells reduce their metabolic flexibility, relying on specific nutrient sources. These cell-specific differences in nutrient utilization should provide insights into the underlying mechanisms of RPE differentiation and diseases.

Methods

Reagent and key resources

All the reagents and key resources were detailed in Supplemental **Table S1** or methods.

Human fRPE cell culture

RPE was isolated from human fetal eye cups and cultured as previously described[11, 16]. The protocol was approved by the Institutional Review Boards of the University of Washington and West Virginia University, and all procedures conform to the ethical principles outlined in the Declaration of Helsinki. Briefly, human fRPE cells were cultured in MEM RPE media, consisting of MEM-α medium supplemented with N1 supplement, non-essential amino acids solution, 1% Fetal Bovine Serum (FBS), and 1% penicillin-streptomycin. (See details in **Table S1**). Cells at passages 4 to 6 were used for experiments, and they were seeded at a density of either 5 x 10^5 cells/cm^2 (regular density) or 4 x 10^5 cells/cm^2 (low density) in 96-well plates. Cell were grown for 4 weeks at regular density or 1-4 weeks at low density to induce dedifferentiation before metabolic screening.

Generation of human iPSC RPE cells

Informed consent was obtained from all subjects prior to inclusion in the study (University of Washington IRB-approved STUDY00010851). Blood drawn from subjects was separated using Ficoll-Hypaque gradient to isolate peripheral blood mononuclear cells. These cells were cultured and reprogrammed using CytoTune Sendai reprogramming kit. Following transfection, cells were cultured on irradiated mouse embryonic fibroblasts until iPSC colonies emerged. Healthy ǂiPSC clones were manually picked and expanded in mTeSR medium on feeder-free plates for cryostorage and differentiation. Karyotyping was performed for all iPSC clones prior to their selection for inclusion in the study.

Generation of SFD patient iPSC RPE and cSFD iPSC RPE cells

SFD iPSC RPE and cSFD iPSC RPE cells were generated as reported[15]. Briefly, following confirmation of iPSC karyotype from SFD patients, iPSC RPE underwent electroporated with Cas9-gRNA (0.75uM, GGGGCCTATTTTCGTAGTAG, Synthego) ribonucleoprotein (RNP) complex and ssDNA donor (4uM, IDT) using Amaxa nucleofector (Human Stem Cell kit 2). Individual iPSC colonies were manually picked

and seeded into 96-well plates. DNA was isolated from each colony and sequenced to identify the gene-edited iPSC colony. To assess potential off-target effects resulting from CRISPR-editing, off-target sites were identified using CRISPOR (http://crispor.tefor.net), which revealed two intronic with three mismatches. These regions were sequenced in the gene-edited iPS RPE, and no genetic alterations were detected[15].

Human iPSC RPE cell culture

iPSC and gene-edited iPSCs were differentiated to RPE in a stepwise procedure as previously described[15]. RPE was maintained in MEM RPE media, detached with 0.25% Trypsin-EDTA and seeded at 5 x 10^5 cells/cm^2 into 96-well plates. RPE cells at passages 4 to 6 were cultured for 4 weeks before metabolic screening.

Human ARPE19 cell culture

Human ARPE19 cells obtained from the American Type Culture Collection (ATCC) were used at passages 5-8 for the experiments. The cells were seeded at 2 x 10^4 cells/cm^2 in 96-well plates and cultured in three different media to mimic dedifferentiated and differentiated states: 1) DMEM/F-12 media with 5% FBS, 2) MEM RPE media, and 3) MEM-NAM (MEM RPE media supplemented with 10 mM NAM as reported[12, 13]. All the ARPE-19 cells were grown for 4 weeks before metabolic screening.

Metabolic screening with metabolic phenotyping microarrays

We used two phenotype microarrays (PM-M1 for carbon sources and PM-M2 for nitrogen sources) (See details in **Table S1**) to assess nutrient utilization. Each well of the 96-well plates contained a specific nutrient except for the negative control (**Table S2-3**). The PM-M1 or PM-M2 plates were initially pre-incubated with 60 uL of nutrient-limiting media (IFM 1, glutamine 200 µM, 1% dialyzed FBS, and 1% penicillin and streptomycin) for one hour. Subsequently, the 96-well plates containing RPE cells underwent two PBS washes before being filled with the pre-incubated nutrients transferred from PM-M1 or PM-M2 microarrays. The plates were then incubated for 40 hours at 37ºC in a 5% CO_2 incubator, after which 10 µL of the redox dye mix MA was added. The plates were sealed and read at an absorbance of 595 nm every 15 minutues for 4 hours.

Statistics

All data are expressed as the mean ± standard deviation. Fold change of absorbance over negative control without nutrient source>1.5, or $p<0.05$ by Student's unpaired two-tailed t-tests using GraphPad Prism 9.0, was considered significant. Heatmaps were generated in Microsoft Excel.

Results

Mature human fRPE cells demonstrate remarkable metabolic flexibility to utilize various nutrient sources.

To study nutrient utilization in mature fRPE cells, we grew fRPE for 4 weeks into maturity with RPE characteristic cobblestone morphology and pigmentation (Supplemental **Fig S1A-C**). The mature RPE cultures were switched into nutrient-limiting media with or without specific nutrient from the PM-M1 plate to screen the utilization of 91 carbon sources (**Fig 1A, Table S2**). Remarkably, mature RPE could utilize 23 carbon sources including sugars, glycolysis intermediates (such as sugar phosphates, lactate, and pyruvate), TCA cycle intermediates, nucleosides, fatty acids and ketone bodies (**Fig 1B-C**). In addition to glucose, mature RPE had the capacity to utilize other sugars such as fructose, mannose, and galactose (**Fig 1B-C**). Nucleosides, containing ribose moiety, can serve as alternative energy sources. Mature RPE could robustly utilize inosine, adenosine and uridine.

Similar to PM-M1 carbon source screening, we evaluated the utilization of 92 nitrogen sources, including 27 amino acids and 60 dipeptides in mature RPE using the PM-M2 plate as illustrated in **Fig 1D**. Mature RPE could metabolize 7 amino acids and 17 dipeptides (**Fig 1E**). Except for methionine and tryptophan, the remaining 5 amino acids (proline, ornithine, glutamine, glutamate, and aspartate) follow a similar metabolic pathway to generate α-ketoglutarate (αKG) or oxoacetate, which serves as fuels for the TCA cycle (**Fig 1E, 1F**). Notably, glutamine, glutamate, aspartate, and proline are also present in the 17 dipeptides. These findings suggest that mature fRPE has remarkable metabolic flexibility, enabling them to effectively utilize diverse nutrient sources to fuel their mitochondrial metabolism (**Fig 1C, 1E**).

Dedifferentiated human fRPE loses metabolic flexibility, primarily relying on sugars and glutamine as their main nutrient sources.

Seeding fRPE at low density induces their dedifferentiation into fibroblast-like phenotype[5]. To understand nutrient utilization in dedifferentiated RPE cells, we seeded fRPE at 10% of regular density and grew for 4 weeks. As expected, these cells transitioned from their characteristic cobblestone structure to a fibroblast-like morphology (**Fig 2A**, Supplemental **Fig S1D-E**). We performed metabolic phenotyping of carbon and nitrogen sources like mature fRPE cells (**Fig 2A**). Compared to mature fRPE, dedifferentiated fRPE utilized substantially fewer nutrients, with only 8 carbon and 6 nitrogen sources. Intriguingly, almost all the carbon sources were sugar and sugar phosphates, while all nitrogen sources contained glutamine (**Fig 2B-C**). These results suggest that dedifferentiated RPE cells lose the ability to utilize multiple nutrient sources such as lactate, fatty acid, ketone bodies and proline. Instead, they become

addicted to consuming sugars and glutamine (**Fig 2D**). We also performed PM-M1 screening on 1-week fRPE with low-density seeding to examine potential changes in nutrient utilization over time (**Fig S2A-B**). Unlike fRPE cells seeded at regular density, those seeded with low density for 1 week displayed a fibroblast-like morphology resembling that of 4-week cultured fRPE cells (**Fig S1D-E**). Nutrient utilization in 1-week cells were largely consistent with those of 4-week fRPE, except for the capability to utilize galactose and adenosine in 1-week cells (**Fig S2B**), suggesting that culture time has minimal impact on metabolic phenotype of nutrient utilization in RPE cells seeded at low density. Consequently, we did not perform PM-M2 screening on 1-week fRPE.

To investigate the mechanism underlying these distinct metabolic phenotypes between mature and dedifferentiated RPE cells, we analyzed the expression of metabolic genes related to nutrient utilization in two RNA-Seq data sets: 1) mature fRPE vs dedifferentiated RPE induced by multiple passages[17] and 2) mature primary adult RPE vs dedifferentiated RPE induced by transforming growth factor-beta (TGFβ) and tumor necrosis factor α (TNFα)[18]. Both dedifferentiated RPE models had significant downregulation of genes invloved in fatty acid oxidation, TCA cycle, transporters for lactate and ketone bodies, nucleotide metabolism, and amino acid metabolism especially proline catabolism and glutamine synthetase (**Table S4, Fig 2E**). These data corroborate our findings that dedifferentiated RPE cannot efficiently utilize fatty acid, lactate, ketone bodies, proline and other nucleosides for mitochondrial metabolism. Importantly, genes involved in proline synthesis, glycolysis, collagen and heparin sulfate were substantially upregulated (**Table S4**), suggesting dedifferentiated RPE cells utilize sugar and glutamine to activate proline synthesis and the hexosamine biosynthetic pathway to produce collagen and glycan for ECM remodeling **(Fig 2E)**.

Human iPSC RPE cells have similar metabolic flexibility to fRPE cells but utilize more sugars and TCA cycle intermediates.

To study nutrient utilization in human iPSC RPE cells, we cultured iPSC RPE for 4 weeks to reach maturity (**Fig S3**) and then replaced media with carbon or nitrogen sources from PM-M1 or PM-M2 for metabolic phenotyping (**Fig 3A**). iPSC RPE could utilize 31 carbon sources and 17 nitrogen sources (**Fig 3B-D**). Similar to fRPE, iPSC RPE demonstrated robust flexibility to utilize various sugars, fatty acids, lactate, ketone bodies, nucleosides, amino acids, and dipeptides (**Fig 3B-D**). However, unlike fRPE, iPSC RPE showed a preference for more sugars and TCA cycle intermediates, but less amino acids and dipeptides (**Fig 3E-F**). These results suggest both healthy fRPE and iPSC RPE posesess metabolic flexiblility to adapt to different substrates, yet also have cell type-specific preferences for certain substrates.

SFD iPSC RPE cells utilize less intermediates from glycolytic and TCA cycle intermediates but more branch-chain amino acids (BCAAs).

We reported SFD iPSC RPE cells harboring the *TIMP3* S204 mutation have increased extracellular deposits and elevated intracellular 4-hydroxyproline[15]. These iPSC RPE and their CRISPR-corrected cSFD were grown into maturity for 4 weeks before undergoing metabolic phenotyping with PM-M1 and PM-M2 (**Fig 4A**). Both SFD and cSFD had normal cobblestone structure and pigmentation (**Fig S4A-B**). While SFD RPE cells utilized 19 carbon sources and 19 nitrogen sources, cSFD RPE cells utilized 28 carbon sources and 7 nitrogen sources (**Fig 4B-E**). Similar to mature fRPE and normal iPSC RPE, SFD RPE utilized different types of sugar, nucleosides, fatty acids, ketone bodies, amino acids and dipeptides (**Fig 4B, 4D**). However, SFD RPE could not utilize lactate, sugar phosphate, short-chain fatty acids (acetate and butyrate), succinate, αKG and gamma-aminobutyric acid (GABA). Notably, the CRISPR-corrected RPE cells restored the utilization of these nutrients (**Fig 4C-E**). SFD RPE could use proline and dipeptides containing glutamine, alanine and arginine. Intriguingly, many of the dipeptides utilized by SFD RPE cells contained BCAAs inlcuding leucine, isoleucine and valine, along with the ability to catabolize free leucine (**Fig 4D**). These metabolic phenotypes are different from fRPE and healthy iPSC RPE cells. While the cSFD RPE cells did not use the BCAAs but they also utilized significantly less nitrogen sources (**Fig 4E, Fig S4C**). These results suggest that SFD RPE cells have metabolic defects in recycling nutrients such as lactate from the neural retina but rely more on BCAAs, which may contribute to the formation of sub-RPE deposits of lipids and ECM proteins (**Fig 4F**).

Culture media composition controls the differentiation and nutrient utilization in APRE19 cells.

ARPE19 cells are typically cultured in DMEM/F-12 media by manufacturer's instruction. However, when ARPE19 cells are cultured in MEM-α-based RPE culture media supplemented with NAM, these cells can undergo rapid differentiatiation into a mature RPE-like phenotype[12, 13]. As a proof of principal that medium composition can influence nutrient utilization in ARPE19 cells, we cultured them into three media (DMEM/F12, MEM RPE media and MEM RPE media plus NAM) for 4 weeks and focused only on the screening of carbon sources using PM-M1 plate (**Fig 5A**). ARPE19 cells in DMEM/F12 had fibroblast-like morphology (**Fig S5A**). MEM RPE media partially differentiated the cell line into RPE-like cobblestone structure with clumps of cells on the top. However, NAM almost completely differentiated APRE-19 cells into mature RPE-like morphology as reported (**Fig S5B-C**). The DMEM/F12 cultured cells could utilize 16 carbon sources including sugar, fatty acids, nucleosides, pyruvate, mono-methyl-succinate and two intermediates from amino acid metabolism (**Fig 5B**). Similar to dedifferentiated fRPE, APRE19 cells cultured in DMEM/F12 could not utilize lactate, ketone bodies and

xylitol (**Fig 5B, Fig 6A**), suggesting a common metabolic defect in dedifferentiated RPE cells. ARPE19 cells cultured in MEM RPE media could utilize 24 carbon sources, which covered 94% of nutrients that were used by DMEM/F12 cultured cells. Cells cultured in MEM RPE media could utilize ketone bodies, glycogen and other sugar, but still could not metabolize lactate and xylitol (**Fig 5C**). The supplementation with NAM enabled ARPE-19 cells to utilize lactate, ketone bodies, sugar phosphate, xylose and tagatose (**Fig 5D-E**), demonstrating patterns similar to those observed in mature fRPE and iPSC RPE, except for the reduced utilization of short-chain fatty acids and maltose (**Fig 6A**). These results further underscore the critical roles of nutrient availability and utilization in RPE differentiation.

Discussion

In this study, we have identified distinctive metabolic phenotypes of nutrient utilization in healthy and diseased human RPE cells (**Fig 6**). Mature fRPE and iPSC RPE are metabolically flexible, capable of adapting to various nutrient sources. Conversely, dedifferentiated RPE cells and SFD patient-derived iPSC RPE cells reduce their flexibility to dependend on specific substrates. Our findings suggest the critical roles of nutrient utilization in RPE differentiation and dedifferentiation.

Every day, RPE must manage a plentiful nutrient influx origninating from phagocytosed lipid- and protein-rich photoreceptor outer segments, from “waste products” such as lactate produced by the neural retina, and rich from nutrient-laden blood through choroid circulation[1, 2]. In addition to direct transport of nutrients to the neural retina, RPE can recycle and generate nutrients via lysosomes and mitochondria to support retinal metabolism, thereby establishing a metabolic ecosystem between the outer retina and RPE[1, 2, 19]. The ability to utilize various nutrients is crucial for maintaining this metabolic ecosystem and disruption of this balance due to mitochondrial and/or lysosomal dysfunction in RPE can lead to retinal degeneration[3, 4, 20]. Healthy human RPE cells are known to be versatile in utilizing different nutrients, including glucose, galactose, lactate, fatty acids, succinate, proline, glutamine and other amino acids[11, 19, 21-24]. Consistent with these findings, our results demonstrate both healthy fRPE and iPSC RPE cells are capable of utilizing these nutrients.

Furthermore, we have found human RPE cells utilize a wide range of other nutrients including various sugars, ketone bodies, nucleosides and dipeptides. Mannose and galactose, for example, are components of glycoproteins found abundantly in the outer segment proteins such as rhodopsin and peripherin 2[25-27]. The ability to utilize these sugars from daily degradation of outer segment may preserve more glucose for the photoreceptors. Additionally, like the liver, human RPE cells can synthesize ketone bodies, which can be utilized by the neural retina[22, 28]. Interestingly, we have found mature human RPE can also readily

utilize ketone bodies but not the dedifferentiated RPE cells, suggesting that the ability to utilizing ketone bodies might be a characteristic of RPE metabolism. Consistent with this metabolic capability, mature RPE expresses key genes involved in ketone bodies degradation[22], a feature distinct from the liver, which can not utilize ketone bodies. Our findings undscore the metabolic flexibility of healthy mature RPE cells in nutrient utilization, an essential RPE function to support retinal metabolism and health.

RPE EMT and dedifferentiation are important events in wound healing and pathogenesis of proliferative vitreoretinopathy and AMD[29]. We have found dedifferentiated RPE cells are unable to utilize alternative fuels like lactate, fatty acids, ketone bodies and proline, but instead, they prefer to utilize sugars and glutamine. RNA-seq data from EMT models show reduced genes in TCA cycle, lactate transport, ketone body utilization and proline catabolism and glutamine synthesis, whereas genes associated in glycolysis, proline synthesis, collagen synthesis and glycoproteins are upregulated (**Fig 2E, Table S4**). Consistently, dedifferentiated RPE cells have been reported to switch from oxidative phosphorylation to glycolysis and lose the ability to utilize proline as a fuel[5, 16]. Inhibition of mitochondrial metabolism in human RPE cells or mouse RPE is sufficient to cause the activation of glycolysis, RPE dedifferentiation and retinal degeneration[4, 30]. Furthermore, mitochondrial respiration diminishes in primarily cultured RPE cells from AMD donors[31]. Inhibiting mitochondrial respiration impedes proline consumption while increasing glucose consumption and lactate production[9]. The inability to utilize exogenous lactate and other alternative nutrient sources in RPE may be an important mechanism in RPE differentiation and AMD pathogenesis.

A key feature in dedifferentiated cells is their massive production of ECM proteins, primarily collagens and glycoproteins, through activating cytokine signaling such as TGFβ and TNFα[32, 33]. In fibroblasts, TGFβ stimulates the oxidation of glucose and glutamine to synthesize proline and other amino acids crucial for ECM protein production[34]. Interestingly, proline synthesis acts as a vent for growth when cells are under mitochondrial redox stress or hypoxia by recycling NADH into NAD^+, thus enhancing the oxidation of glutamine and glucose[34, 35]. Proline synthesis may be particularly crucial for dedifferentiated RPE cells, given their inhibited mitochondrial metabolism and heavy reliance on lactate production for NAD^+ regeneration. Strategies aimed at relieving mitochondrial redox stress and reverting proline synthesis to proline catabolism could hold promise for treating RPE dedifferentiation.

TIMP3, a risk gene for AMD, is secreted by the RPE and plays a critical role in ECM remodeling by inhibiting matrix metalloproteinases[36]. Mutations in *TIMP3* cause SFD, characterized by drusen-like sub-RPE deposits containing lipids and ECM proteins[15, 37]. Unlike healthy or mutation-corrected RPE cells,

SFD RPE cells utilize more free BCAAs or dipeptides containing BCAAs (**Fig 4F, Fig 6**). BCAAs are ketogenic amino acids and their oxidation promotes the synthesis and transport of fatty acids and cholesterol[38, 39]. BCAA oxidation is closely associated with dysregulated glucose and lipid metabolism in diabetes and non-alcoholic fatty liver diseases[38, 40, 41]. Interestingly, intermediates of the BCAA degradation pathway are significantly elevated in the plasma of AMD patients[42], and *BCAT1*, a key gene in BCAA degradation, upregulates in the RPE/choroid from AMD donors[43]. Moreover, in addition to proline, ECM proteins are highly enriched with BCAAs[44] . Our findings suggest that SFD RPE might upregulate BCAA degradation pathway by utilizing BCAAs from free amino acids or protein degradation, contributing to the formation of their sub-RPE deposits.

In conclusion, metabolic phenotyping offers a sensitive and powerful platform for measuring nutrient utilization in healthy and diseased human RPE cells. Healthy and mature human fRPE and iPSC RPE have similar features of high metabolic flexibility in utilizing various nutrient sources. However, dedifferentiated RPE or SFD RPE cells demonstrate selective preferences, favoring the use of sugars, glutamine or BCAAs, which may contribute to their morphological and pathological alterations in AMD and SFD.

Acknowledgment

This work was supported by National Institutes of Health Grant EY034364 (J. R. C. and J. D), EY03459 (J. R. C. and J. D), EY031324 (JD), EY032462(JD), the Retina Research Foundation (JD), Human Development grant R24HD000836 (The Birth Defects Research Laboratory from the University of Washington), and funds for Core facilities P20 GM103434 and P20 GM144230 (WV INBRE grant).

Conflicts of interest

The authors declare no conflicts of interest.

References

1. Lakkaraju A, Umapathy A, Tan LX, et al. The cell biology of the retinal pigment epithelium. *Prog Retin Eye Res* 2020;100846.
2. Hurley JB. Retina Metabolism and Metabolism in the Pigmented Epithelium: A Busy Intersection. *Annu Rev Vis Sci* 2021;7:665-692.
3. Ferrington DA, Fisher CR, Kowluru RA. Mitochondrial Defects Drive Degenerative Retinal Diseases. *Trends Mol Med* 2020;26:105-118.

376 4. Zhao C, Yasumura D, Li X, et al. mTOR-mediated dedifferentiation of the retinal pigment
377 epithelium initiates photoreceptor degeneration in mice. *J Clin Invest* 2011;121:369-383.
378 5. Adijanto J, Philp NJ. Cultured primary human fetal retinal pigment epithelium (hfRPE) as a model
379 for evaluating RPE metabolism. *Exp Eye Res* 2014;126:77-84.
380 6. Bharti K, den Hollander AI, Lakkaraju A, et al. Cell culture models to study retinal pigment
381 epithelium-related pathogenesis in age-related macular degeneration. *Exp Eye Res* 2022;222:109170.
382 7. Nazari H, Zhang L, Zhu D, et al. Stem cell based therapies for age-related macular degeneration:
383 The promises and the challenges. *Prog Retin Eye Res* 2015;48:1-39.
384 8. Blenkinsop TA, Saini JS, Maminishkis A, et al. Human Adult Retinal Pigment Epithelial Stem Cell-
385 Derived RPE Monolayers Exhibit Key Physiological Characteristics of Native Tissue. *Invest Ophthalmol Vis*
386 *Sci* 2015;56:7085-7099.
387 9. Zhang R, Engel AL, Wang Y, et al. Inhibition of Mitochondrial Respiration Impairs Nutrient
388 Consumption and Metabolite Transport in Human Retinal Pigment Epithelium. *J Proteome Res*
389 2021;20:909-922.
390 10. Du J, Zhu S, Lim RR, Chao JR. Proline metabolism and transport in retinal health and disease.
391 *Amino Acids* 2021;53:1789-1806.
392 11. Chao JR, Knight K, Engel AL, et al. Human retinal pigment epithelial cells prefer proline as a
393 nutrient and transport metabolic intermediates to the retinal side. *J Biol Chem* 2017;292:12895-12905.
394 12. Hazim RA, Volland S, Yen A, Burgess BL, Williams DS. Rapid differentiation of the human RPE cell
395 line, ARPE-19, induced by nicotinamide. *Exp Eye Res* 2019;179:18-24.
396 13. Hazim RA, Paniagua AE, Tang L, et al. Vitamin B3, nicotinamide, enhances mitochondrial
397 metabolism to promote differentiation of the retinal pigment epithelium. *J Biol Chem* 2022;298:102286.
398 14. Anand-Apte B, Chao JR, Singh R, Stohr H. Sorsby fundus dystrophy: Insights from the past and
399 looking to the future. *J Neurosci Res* 2019;97:88-97.
400 15. Engel AL, Wang Y, Khuu TH, et al. Extracellular matrix dysfunction in Sorsby patient-derived
401 retinal pigment epithelium. *Exp Eye Res* 2022;215:108899.
402 16. Yam M, Engel AL, Wang Y, et al. Proline mediates metabolic communication between retinal
403 pigment epithelial cells and the retina. *J Biol Chem* 2019;294:10278-10289.
404 17. Radeke MJ, Radeke CM, Shih YH, et al. Restoration of mesenchymal retinal pigmented epithelial
405 cells by TGFbeta pathway inhibitors: implications for age-related macular degeneration. *Genome Med*
406 2015;7:58.
407 18. Boles NC, Fernandes M, Swigut T, et al. Epigenomic and Transcriptomic Changes During Human
408 RPE EMT in a Stem Cell Model of Epiretinal Membrane Pathogenesis and Prevention by Nicotinamide.
409 *Stem Cell Reports* 2020;14:631-647.
410 19. Kanow MA, Giarmarco MM, Jankowski CS, et al. Biochemical adaptations of the retina and
411 retinal pigment epithelium support a metabolic ecosystem in the vertebrate eye. *Elife* 2017;6.
412 20. Boya P, Kaarniranta K, Handa JT, Sinha D. Lysosomes in retinal health and disease. *Trends*
413 *Neurosci* 2023;46:1067-1082.
414 21. Liu B, Calton MA, Abell NS, et al. Genetic analyses of human fetal retinal pigment epithelium
415 gene expression suggest ocular disease mechanisms. *Commun Biol* 2019;2:186.
416 22. Adijanto J, Du J, Moffat C, Seifert EL, Hurle JB, Philp NJ. The retinal pigment epithelium utilizes
417 fatty acids for ketogenesis. *J Biol Chem* 2014;289:20570-20582.
418 23. Bisbach CM, Hass DT, Robbings BM, et al. Succinate Can Shuttle Reducing Power from the
419 Hypoxic Retina to the O(2)-Rich Pigment Epithelium. *Cell Rep* 2020;31:107606.
420 24. Li B, Zhang T, Liu W, et al. Metabolic Features of Mouse and Human Retinas: Rods versus Cones,
421 Macula versus Periphery, Retina versus RPE. *iScience* 2020;23:101672.
422 25. Skiba NP, Lewis TR, Spencer WJ, Castillo CM, Shevchenko A, Arshavsky VY. Absolute
423 Quantification of Photoreceptor Outer Segment Proteins. *J Proteome Res* 2023;22:2703-2713.

26. Stuck MW, Conley SM, Naash MI. PRPH2/RDS and ROM-1: Historical context, current views and future considerations. *Prog Retin Eye Res* 2016;52:47-63.
27. Daniele LL, Han JYS, Samuels IS, et al. Glucose uptake by GLUT1 in photoreceptors is essential for outer segment renewal and rod photoreceptor survival. *FASEB J* 2022;36:e22428.
28. Reyes-Reveles J, Dhingra A, Alexander D, Bragin A, Philp NJ, Boesze-Battaglia K. Phagocytosis-dependent ketogenesis in retinal pigment epithelium. *J Biol Chem* 2017;292:8038-8047.
29. Zhou M, Geathers JS, Grillo SL, et al. Role of Epithelial-Mesenchymal Transition in Retinal Pigment Epithelium Dysfunction. *Front Cell Dev Biol* 2020;8:501.
30. Hu X, Calton MA, Tang S, Vollrath D. Depletion of Mitochondrial DNA in Differentiated Retinal Pigment Epithelial Cells. *Sci Rep* 2019;9:15355.
31. Fisher CR, Ferrington DA. Perspective on AMD Pathobiology: A Bioenergetic Crisis in the RPE. *Invest Ophthalmol Vis Sci* 2018;59:AMD41-AMD47.
32. Scott LE, Weinberg SH, Lemmon CA. Mechanochemical Signaling of the Extracellular Matrix in Epithelial-Mesenchymal Transition. *Front Cell Dev Biol* 2019;7:135.
33. Shu DY, Butcher E, Saint-Geniez M. EMT and EndMT: Emerging Roles in Age-Related Macular Degeneration. *Int J Mol Sci* 2020;21.
34. Schworer S, Berisa M, Violante S, et al. Proline biosynthesis is a vent for TGFbeta-induced mitochondrial redox stress. *EMBO J* 2020;39:e103334.
35. Westbrook RL, Bridges E, Roberts J, et al. Proline synthesis through PYCR1 is required to support cancer cell proliferation and survival in oxygen-limiting conditions. *Cell Rep* 2022;38:110320.
36. Alexander JP, Bradley JM, Gabourel JD, Acott TS. Expression of matrix metalloproteinases and inhibitor by human retinal pigment epithelium. *Invest Ophthalmol Vis Sci* 1990;31:2520-2528.
37. Weber BH, Vogt G, Pruett RC, Stohr H, Felbor U. Mutations in the tissue inhibitor of metalloproteinases-3 (TIMP3) in patients with Sorsby's fundus dystrophy. *Nat Genet* 1994;8:352-356.
38. Neinast MD, Jang C, Hui S, et al. Quantitative Analysis of the Whole-Body Metabolic Fate of Branched-Chain Amino Acids. *Cell Metab* 2019;29:417-429 e414.
39. Jang C, Oh SF, Wada S, et al. A branched-chain amino acid metabolite drives vascular fatty acid transport and causes insulin resistance. *Nat Med* 2016;22:421-426.
40. White PJ, McGarrah RW, Grimsrud PA, et al. The BCKDH Kinase and Phosphatase Integrate BCAA and Lipid Metabolism via Regulation of ATP-Citrate Lyase. *Cell Metab* 2018;27:1281-1293 e1287.
41. White PJ, Lapworth AL, An J, et al. Branched-chain amino acid restriction in Zucker-fatty rats improves muscle insulin sensitivity by enhancing efficiency of fatty acid oxidation and acyl-glycine export. *Mol Metab* 2016;5:538-551.
42. Haijes HA, Jans JJM, van der Ham M, van Hasselt PM, Verhoeven-Duif NM. Understanding acute metabolic decompensation in propionic and methylmalonic acidemias: a deep metabolic phenotyping approach. *Orphanet J Rare Dis* 2020;15:68.
43. Newman AM, Gallo NB, Hancox LS, et al. Systems-level analysis of age-related macular degeneration reveals global biomarkers and phenotype-specific functional networks. *Genome Med* 2012;4:16.
44. Li P, Wu G. Roles of dietary glycine, proline, and hydroxyproline in collagen synthesis and animal growth. *Amino Acids* 2018;50:29-38.

Figure legends

Figure 1. Metabolic phenotyping of mature human fRPE cells. (A) A schematic for metabolic phenotyping with carbon sources. Human fRPE cells were grown for 4 weeks in a 96-well plate and then switched into nutrient-limiting media containing different carbon sources in each well from PM-M1 plate.

The utilization of nutrients leads to NADH production, casuing a color change in a redox sensitive dye to purple, which is quantified by a microplate reader at 595 nm. (B) The utilization of carbon sources by mature human fRPE cells and (C) an illustration of the metabolic pathways. (D) A schematic for metabolic phenotyping of nitrogen sources using PM-M2. (E) The utilization of nitrogen sources by mature human fRPE cells and (F) an illustration of the metabolic pathways. N=3. Fold change over negative control without nutrient source (Ctr)>1.5 or *P<0.05 over Ctr. Gluc, Glucose, Gal, galactose; Mann, Mannose; F1P, fructose 1-phosphophate; R1P, ribose 1-phosphate, G6P, glucose 3-phosphate; G3P, glycerol 3-phosphate; AcAc, Acetoacetic Acid; 3HB, β-Hydroxy Butyrate; MelA, Melibionic Acid.

Figure 2. **Metabolic phenotyping of dedifferentiated human fRPE.** (A) Human fRPE were seeded low density to induce dedifferentiation with a mesenchymal phenotype in a 96-well plate and then switched into nutrient-limiting media containing different carbon (PM-M1) or nitrogen sources (PM-M2) for metabolic phenotyping. (B) Nutrient utilization of carbon sources by dedifferentiated human fRPE. N=4. Fold change>1.5 or P<0.05 over Ctr. (C) Nutrient utilization of nitrogen sources by dedifferentiated human fRPE. N=3. Fold change>1.5 or P<0.05 over Ctr. (D) A comparison of metabolic phenotyping between mature fRPE and dedifferentiated fRPE. (E) The dedifferentiated RPE cells lose the ability to utilize multiple nutrient sources but switch to use glutamine, enhancing proline and collagen synthesis. Magenta denotes an increase and blue denotes a decrease in gene expression or metabolic pathways. *PFKFB4*, 6-phosphofructo-2-kinase/fructose-2,6-bisphosphatase 4, *LDHA*, Lactate dehydrogenase A; *OGDH*, Oxoglutarate dehydrogenase; *PRODH*; Proline dehydrogenase; *PYCR1*, Pyrroline-5-carboxylate reductase 1; P4H4, Prolyl 4-hydroxylase subunit alpha or beta; *GMPPA*, GDP-mannose pyrophosphorylase A. *PMM2*, Phosphomannomutase 2.

Figure 3. Metabolic phenotyping of healthy human iPSC RPE cells. (A) Human iPSC RPE cells were differentiated in RPE media for 4 weeks and switched into nutrient-limit media from PM1 or PM2 for metabolic phenotyping. (B-D) Nutrient utilization of carbon sources and nitrogen sources by human iPSC RPE cells. N=3. Fold change>1.5 or P<0.05 over Ctr. (E) A comparison of number of nutrients that were utilized between fRPE and iPSC RPE cells. (F) An illustration of nutrient utilization in iPSC RPE cells. GlcNAc, N-Acetyl-D-Glucosamine; Tcba, Tricarballylic Acid; AlaN, L-Alaninamide.

Figure 4. Metabolic phenotyping of IPSC SFD and cSFD RPE cells. (A) Human iPSC SFD RPE carring TIMP3 204C mutation and mutation corrected cSFD RPE cells were differentiated in RPE media for 4 weeks and then switched to nutrient-limit media with carbon or nitrogen sources from PM-M1 or

PM-M2 for metabolic phenotyping. (B-E) Nutrient utilization of (B-C) carbon sources and (D-E) nitrogen sources in iPSC SFD RPE cells. N=3. Fold change>1.5 or P<0.05 over Ctr. (F) An illustration of altered nutrient utilization in SFD iPSC RPE cells. L-Mal, L-Malic Acid; mmSuc, mono methyl succinate; 3HB, β-Hydroxy Butyrate; BCAAs, Branch-Chained Amino Acids.

Figure 5. Metabolic phenotyping of ARPE19 cells cultured in different media.
(A) ARPE19 cells were cultured in three different media: DMEM/F-12, MEM RPE media, and MEM RPE media with 10 mM NAM for 4 weeks. All the cells were then changed into nutrient-limit media with carbon sources from PM-M1 for metabolic phenotyping. (B-D) Nutrient utilization of carbon sources of ARPE19 cells cultured in (B) DMEM/F12 (C) MEM RPE media, (D) MEM RPE media with NAM. Fold change>1.5 or P<0.05 over Ctr. (E) A comparison of number of nutrients that were utilized in ARPE19 cells grown in different culture media. (F-G) An illustration of altered nutrient utilization in APRE19 cells cultured between DMEM/F12 and MEM RPE media with NAM. Meso-Tar, Meso Tartatic acid; mmSuc, mono methyl succinate; AcAc, Acetoacetic Acid; 3HB, β-Hydroxy Butyrate.

Figure 6. Comparison of metabolic phenotyping profiles of human fRPE cells, dedifferentiated fRPE, iPSC RPE cells, SFD RPE, cSFD RPE and ARPE-19 cells grown under different culture media. Heat map visualization of nutrients that were differentially utilized by different RPE cells from (A) PM-M1 nutrients and (B) PM-M2 nutrient microarray plates. De-fRPE, dedifferentied fRPW with low density seedings; ARPE, ARPE19 cells; MelA, Melibionic Acid; GlcNAc, N-Acetyl-D-Glucosamine; Tcba, Tricarballylic acid; mmSuc, mono methyl succinate; AlaN, Alaninamide.

538 **Figure 1**

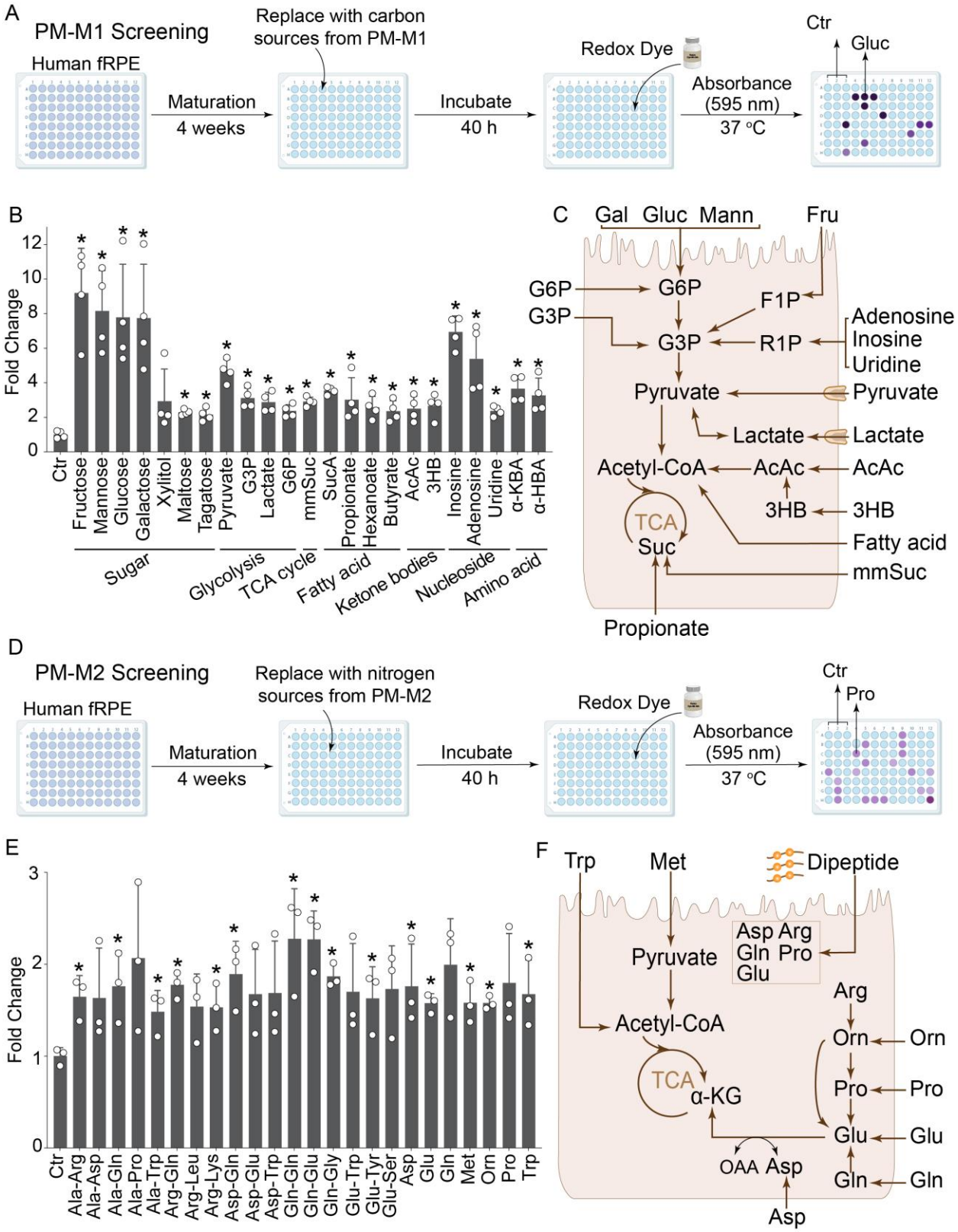

539

Figure 2

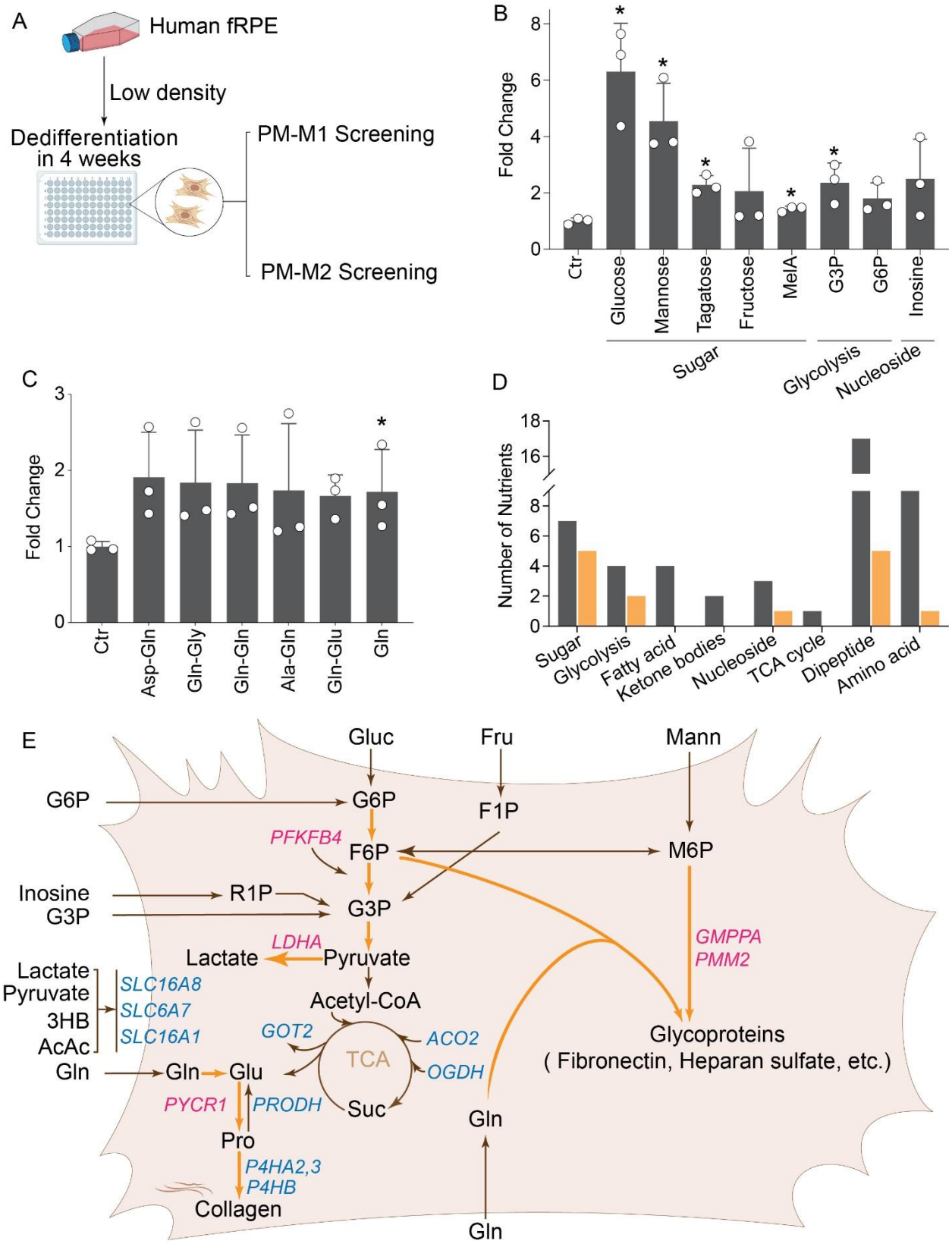
A
Human fRPE
Low density
Dedifferentiation in 4 weeks
PM-M1 Screening
PM-M2 Screening
B
Fold Change
Ctr
Glucose
Mannose
Tagatose
Fructose
MelA
G3P
G6P
Inosine
Sugar
Glycolysis
Nucleoside
C
Fold Change
Ctr
Asp-Gln
Gln-Gly
Gln-Gln
Ala-Gln
Gln-Glu
Gln
D
Number of Nutrients
Sugar
Glycolysis
Fatty acid
Ketone bodies
Nucleoside
TCA cycle
Dipeptide
Amino acid
E
Gluc
Fru
Mann
G6P
F1P
PFKFB4
F6P
M6P
Inosine
R1P
G3P
LDHA
Lactate
Pyruvate
GMPPA
PMM2
Lactate
Pyruvate
3HB
AcAc
SLC16A8
SLC6A7
SLC16A1
Acetyl-CoA
GOT2
ACO2
TCA
OGDH
Glycoproteins
(Fibronectin, Heparan sulfate, etc.)
Gln
Glu
PYCR1
PRODH
Suc
Gln
Pro
P4HA2,3
P4HB
Collagen
Gln

Figure 3

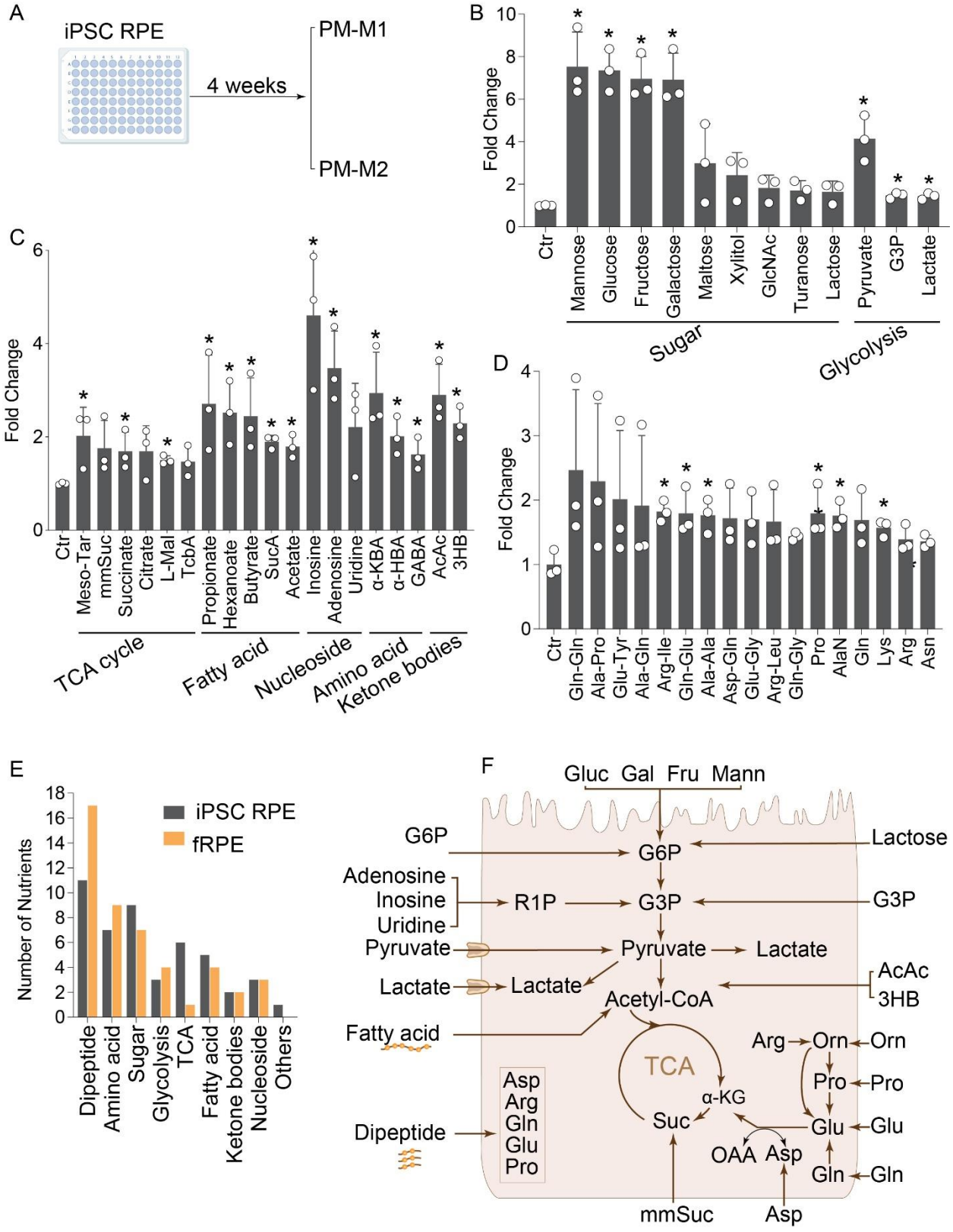
A
iPSC RPE
4 weeks
PM-M1
PM-M2
B
Fold Change
Ctr
Mannose
Glucose
Fructose
Galactose
Maltose
Xylitol
GlcNAc
Turanose
Lactose
Pyruvate
G3P
Lactate
Sugar
Glycolysis
C
Fold Change
Ctr
Meso-Tar
mmSuc
Succinate
Citrate
L-Mal
TcbA
Propionate
Hexanoate
Butyrate
SucA
Acetate
Inosine
Adenosine
Uridine
α-KBA
α-HBA
GABA
AcAc
3HB
TCA cycle
Fatty acid
Nucleoside
Amino acid
Ketone bodies
D
Fold Change
Ctr
Gln-Gln
Ala-Pro
Glu-Tyr
Ala-Gln
Arg-Ile
Gln-Glu
Ala-Ala
Asp-Gln
Glu-Gly
Arg-Leu
Gln-Gly
Pro
AlaN
Gln
Lys
Arg
Asn
E
Number of Nutrients
iPSC RPE
fRPE
Dipeptide
Amino acid
Sugar
Glycolysis
TCA
Fatty acid
Ketone bodies
Nucleoside
Others
F
Gluc Gal Fru Mann
G6P
Lactose
G6P
Adenosine
Inosine
Uridine
R1P
G3P
G3P
Pyruvate
Pyruvate
Lactate
Lactate
Lactate
AcAc
3HB
Acetyl-CoA
Fatty acid
Arg
Orn
Orn
TCA
Pro
Pro
α-KG
Asp
Arg
Gln
Glu
Pro
Suc
Glu
Glu
Dipeptide
OAA
Asp
Gln
Gln
mmSuc
Asp

Figure 4

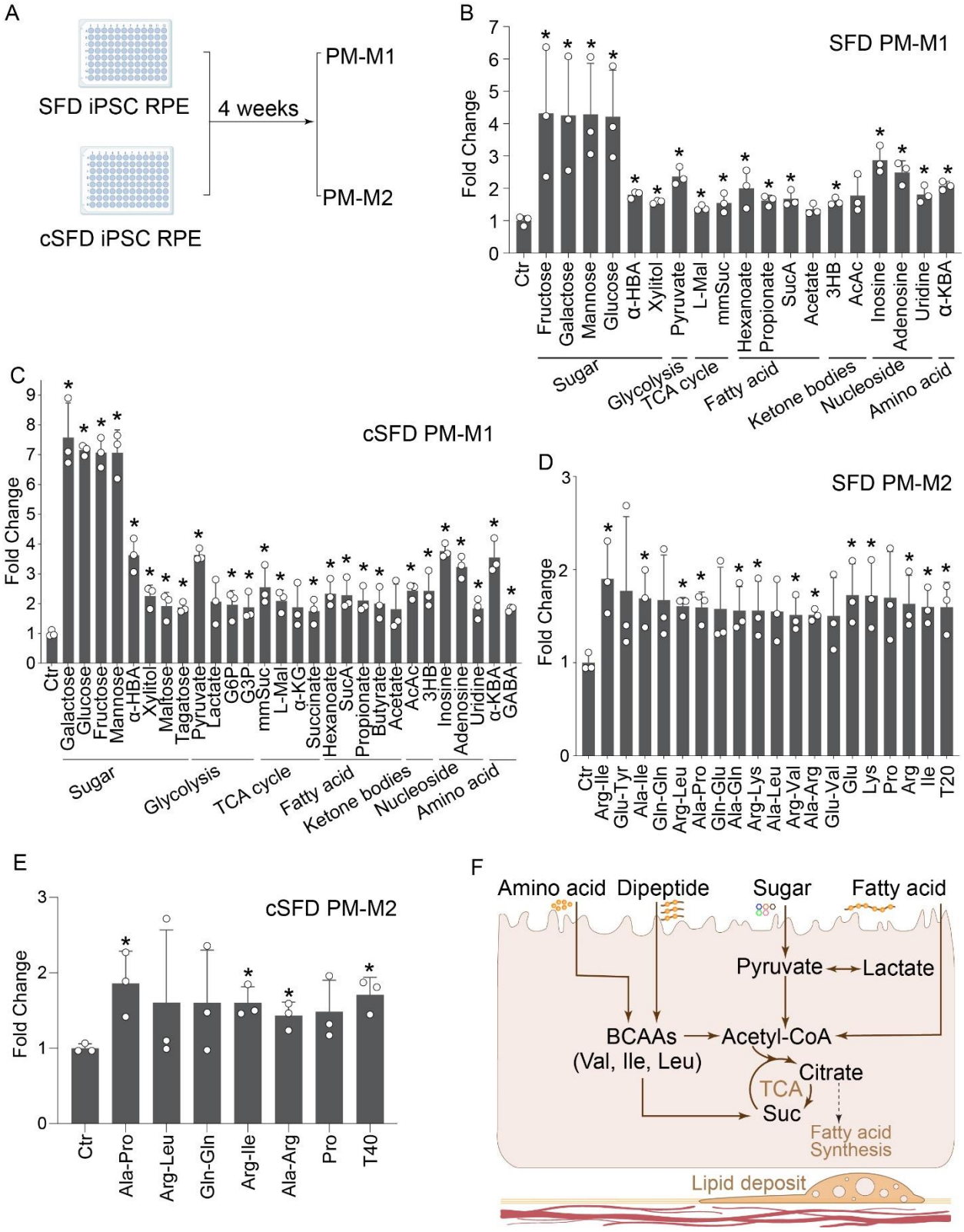
A
SFD iPSC RPE
cSFD iPSC RPE
4 weeks
PM-M1
PM-M2
B
SFD PM-M1
Fold Change
Ctr
Fructose
Galactose
Mannose
Glucose
α-HBA
Xylitol
Pyruvate
L-Mal
mmSuc
Hexanoate
Propionate
SucA
Acetate
3HB
AcAc
Inosine
Adenosine
Uridine
α-KBA
Sugar
Glycolysis
TCA cycle
Fatty acid
Ketone bodies
Nucleoside
Amino acid
C
cSFD PM-M1
Fold Change
Ctr
Galactose
Glucose
Fructose
Mannose
α-HBA
Xylitol
Maltose
Tagatose
Pyruvate
Lactate
G6P
G3P
mmSuc
L-Mal
α-KG
Succinate
Hexanoate
SucA
Propionate
Butyrate
Acetate
AcAc
3HB
Inosine
Adenosine
Uridine
α-KBA
GABA
Sugar
Glycolysis
TCA cycle
Fatty acid
Ketone bodies
Nucleoside
Amino acid
D
SFD PM-M2
Fold Change
Ctr
Arg-Ile
Glu-Tyr
Ala-Ile
Gln-Gln
Arg-Leu
Ala-Pro
Gln-Glu
Ala-Gln
Arg-Lys
Ala-Leu
Arg-Val
Ala-Arg
Glu-Val
Glu
Lys
Pro
Arg
Ile
T20
E
cSFD PM-M2
Fold Change
Ctr
Ala-Pro
Arg-Leu
Gln-Gln
Arg-Ile
Ala-Arg
Pro
T40
F
Amino acid
Dipeptide
Sugar
Fatty acid
Pyruvate
Lactate
BCAAs
(Val, Ile, Leu)
Acetyl-CoA
Citrate
TCA
Suc
Fatty acid
Synthesis
Lipid deposit

548 **Figure 5**

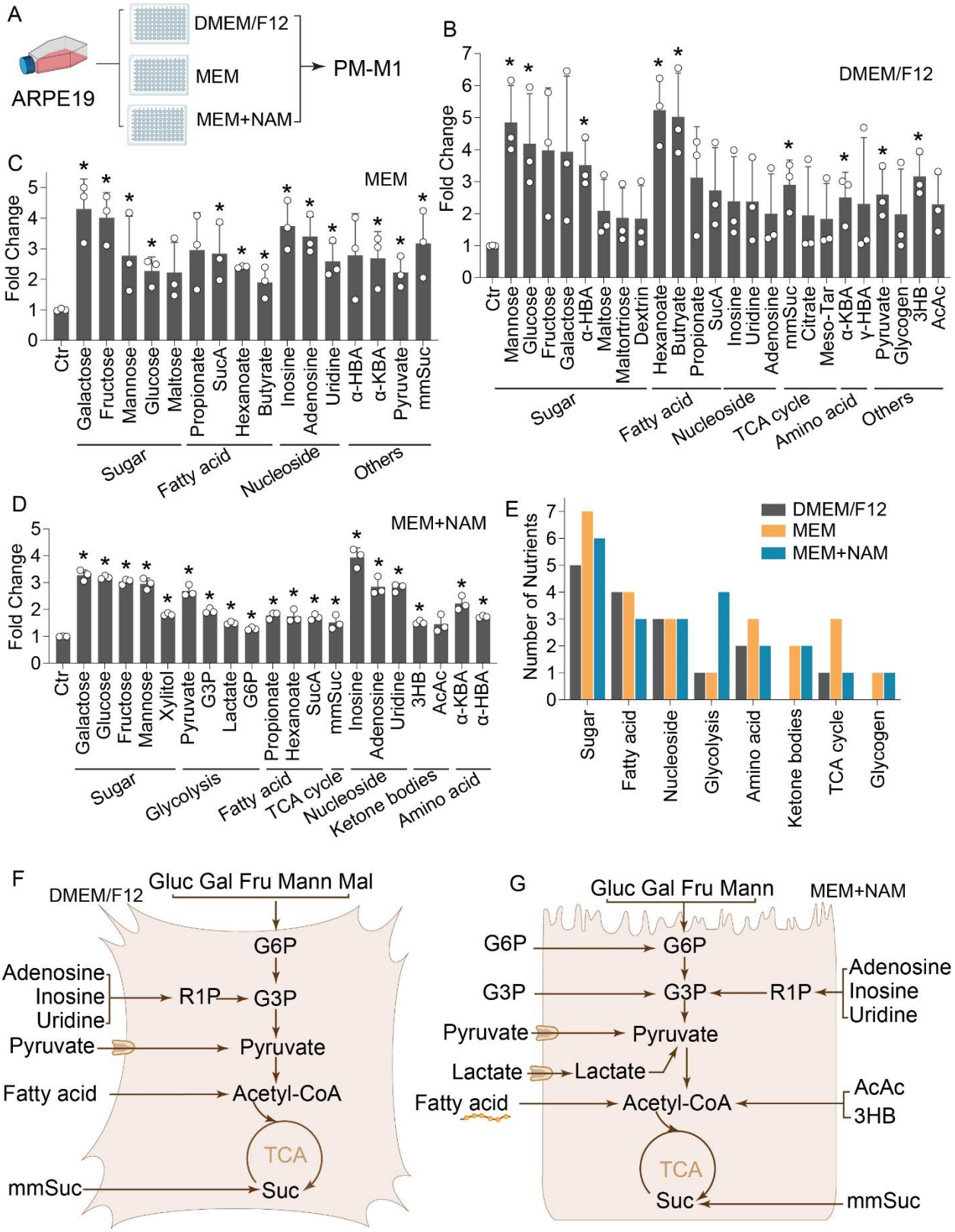

549

550

Figure 6

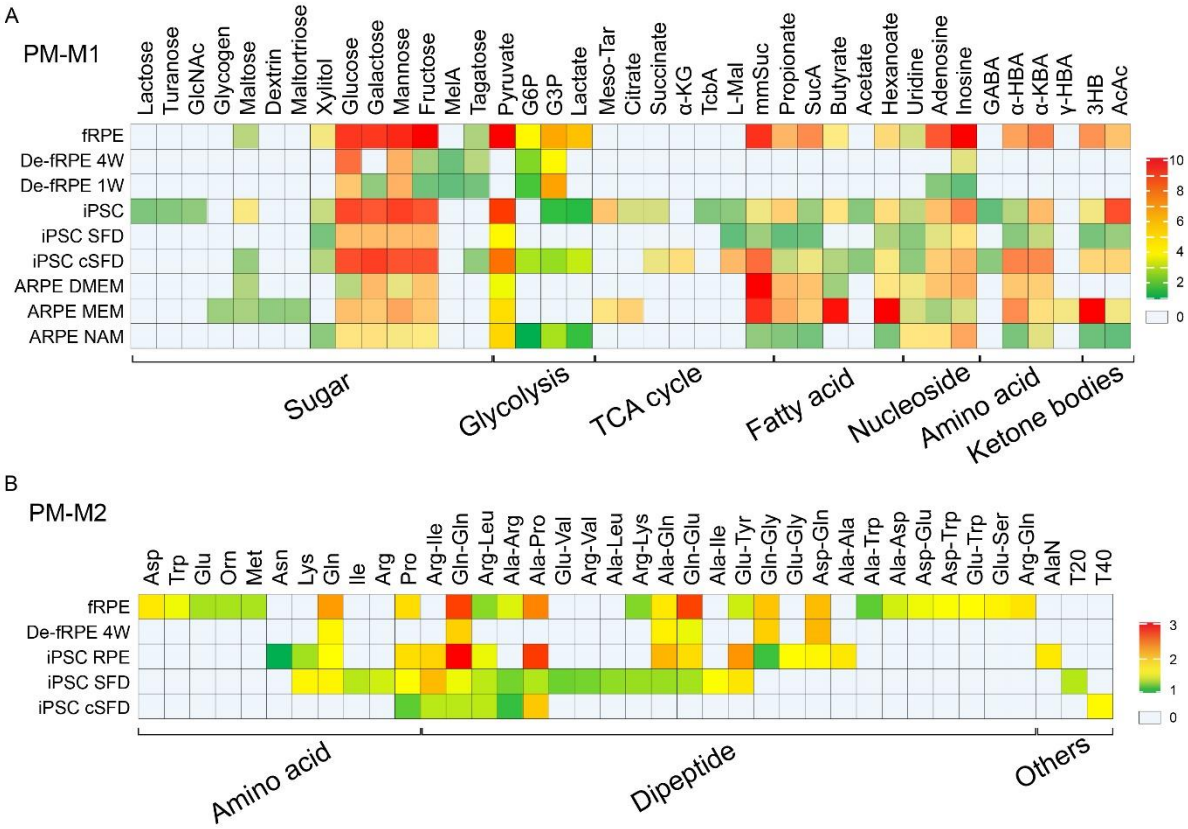
A
PM-M1
Lactose
Turanose
GlcNAc
Glycogen
Maltose
Dextrin
Maltortriose
Xylitol
Glucose
Galactose
Mannose
Fructose
MelA
Tagatose
Pyruvate
G6P
G3P
Lactate
Meso-Tar
Citrate
Succinate
α-KG
TcbA
L-Mal
mmSuc
Propionate
SucA
Butyrate
Acetate
Hexanoate
Uridine
Adenosine
Inosine
GABA
α-HBA
α-KBA
γ-HBA
3HB
AcAc
fRPE
De-fRPE 4W
De-fRPE 1W
iPSC
iPSC SFD
iPSC cSFD
ARPE DMEM
ARPE MEM
ARPE NAM
10
8
6
4
2
0
Sugar
Glycolysis
TCA cycle
Fatty acid
Nucleoside
Amino acid
Ketone bodies
B
PM-M2
Asp
Trp
Glu
Orn
Met
Asn
Lys
Gln
Ile
Arg
Pro
Arg-Ile
Gln-Gln
Arg-Leu
Ala-Arg
Ala-Pro
Glu-Val
Arg-Val
Ala-Leu
Arg-Lys
Ala-Gln
Gln-Glu
Ala-Ile
Glu-Tyr
Gln-Gly
Glu-Gly
Asp-Gln
Ala-Ala
Ala-Trp
Ala-Asp
Asp-Glu
Asp-Trp
Glu-Trp
Glu-Ser
Arg-Gln
AlaN
T20
T40
fRPE
De-fRPE 4W
iPSC RPE
iPSC SFD
iPSC cSFD
3
2
1
0
Amino acid
Dipeptide
Others